THE JOURNAL OF PHYSICAL CHEMISTRY B

Article

pubs.acs.org/JPCB

Molecular Driving Forces behind the Tetrahydrofuran–Water Miscibility Gap

Micholas Dean Smith,[†,‡] Barmak Mostofian,[†,§] Loukas Petridis,[†] Xiaolin Cheng,[†] and Jeremy C. Smith*[,†,‡]

[†]Center for Molecular Biophysics, University of Tennessee and Oak Ridge National Laboratory, Oak Ridge, Tennessee 37830, United States

[‡]Department of Biochemistry and Cellular Molecular Biology, University of Tennessee, M407 Walters Life Sciences, 1414 Cumberland Avenue, Knoxville, Tennessee 37996, United States

[§]Joint Institute for Biological Sciences, University of Tennessee and Oak Ridge National Laboratory, Oak Ridge, Tennessee 37830, United States

Supporting Information

ABSTRACT: The tetrahydrofuran–water binary system exhibits an unusual closed-loop miscibility gap (transitions from a miscible regime to an immiscible regime back to another miscible regime as the temperature increases). Here, using all-atom molecular dynamics simulations, we probe the structural and dynamical behavior of the binary system in the temperature regime of this gap at four different mass ratios, and we compare the behavior of bulk water and tetrahydrofuran. The changes in structure and dynamics observed in the simulations indicate that the temperature region associated with the miscibility gap is distinctive. Within the miscibility-gap temperature region, the self-diffusion of water is significantly altered and the second virial coefficients (pair-interaction strengths) show parabolic-like behavior. Overall, the results suggest that the gap is the result of differing trends with temperature of minor structural changes, which produces interaction virials with parabolic temperature dependence near the miscibility gap.

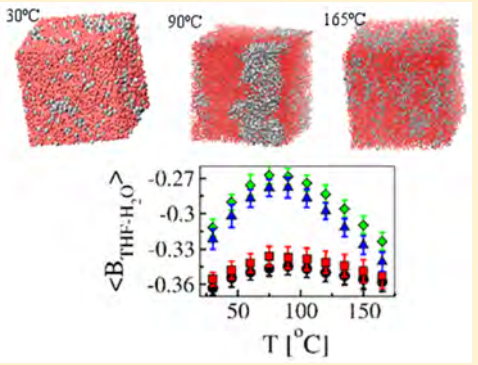

INTRODUCTION

Tetrahydrofuran (THF) is a ubiquitous organic solvent. Its uses range from liquid-phase chromatography[1] and organic synthesis to polymer chemistry.[2−4] Of particular recent interest is the finding that aqueous solutions of THF readily dissolve lignocellulosic biomass, resulting in greatly increased yields of biofuel precursor molecules.[5,6]

At temperatures between 60 and 145 °C and THF/H_2O mass ratios between 0.3 and 2.8, THF–water solutions enter a closed-loop "miscibility gap", where closed loop means that the system is miscible at temperatures below a threshold, becomes immiscible, and then becomes miscible again at a higher temperature.[7] The presence of this immiscible region is a peculiar feature, as it is found at a variety of THF/water ratios and over a wide range of temperatures.[7,8] The miscibility gap has been described as leading to the solution going from transparent to cloudy.[8] The molecular mechanism behind this phase separation is of interest, and as such, determination of the structural and dynamical properties of the binary system over a variety of temperatures would be intriguing.

From available experimental work, a variety of structure and structure-related properties of THF–water solutions have been deduced. These include neutron diffraction-derived radial distribution functions,[9,10] a negative volume of mixing,[11] the existence of THF–water hydrogen bonds,[9,10,12] nanometer-scale phase separation[13] in the miscible temperature regime, the presence of voids,[9,10,13] a preferred T-like orientation for groupings of THF molecules,[9,10] and the presence of smooth changes in the dielectric constant of the solution with increasing concentrations of THF[14] (at temperatures and pressures below the immiscible region). Although this substantial amount of data is useful, unfortunately nearly all of it was determined only for the miscible regime. Therefore, one would ideally perform the same experiments again in the immiscible region, to complete our picture of the THF–water system. However, this has proved challenging, as the existence of the closed-loop gap is extremely sensitive to contamination. Further, isotope substitution, with regard to THF, removes the immiscible region,[7,15,16] allowing only an incomplete picture from neutron diffraction in the two-phase region.

Given the experimental difficulties with probing the immiscible region, computer simulations become particularly important to deploy. To date, only one simulation[17] of the THF–water system in the immiscible region has been performed, which made use of the Gibbs ensemble Monte Carlo technique and provided an approximate coexistence curve as well as some measures of structure (OW–OW radial distribution functions, THF–hydrogen to water–oxygen radial

Received: October 6, 2015
Revised: December 30, 2015
Published: January 6, 2016

DOI: 10.1021/acs.jpcb.5b09770
J. Phys. Chem. B 2016, 120, 740−747

distributions, equilibrium hydrogen-bond numbers, and center-of-mass radial distribution functions) and a water-cluster analysis.[18] Although these early simulations have resolved much of the structure of the phase-separated THF−water system, the molecular mechanisms by which the gap forms are not clear. To begin to address this, we perform classical molecular dynamics (MD) simulations of the binary system at temperatures below, within, and above the experimental miscibility gap, and we examine the structural and dynamical features of the system prior to complete phase separation. We characterize the behavior over 10 different temperatures and six different THF/water mass ratios by examining the center-of-mass radial distribution functions, different coordination pairs, hydrogen-bond frequencies and lifetimes, and the diffusion behavior of each species. Furthermore, we compute the second virial coefficient/pair interaction strengths (and its constituent decomposition) of the system at each temperature and concentration. The calculations reveal significant changes related to THF and water dynamics and nonmonotonic behavior of the second virial coefficient/pair interaction strengths within and near the immiscible region.

COMPUTATIONAL METHODOLOGY

Simulation Details. All-atom molecular dynamics simulations using the CHARMM32[19] force-field parametrization were performed at 10 different temperatures (30−165 °C in 15 °C increments) with six different mass ratios of THF to TIP3P[20] water [bulk water, bulk THF, 0.3 THF/H_2O (m/m), 0.4 THF/H_2O (m/m), 0.89 THF/H_2O (m/m), and 1.5 THF/H_2O (m/m); see Table 1 for a summary of system sizes]. At each mass ratio, the number of atoms was on the order of ∼5000. This number of atoms was chosen to be small so that the system would not be able to undergo a possible complete phase separation,[21,22] which in turn affords us the ability to sufficiently sample the preseparation configurational space and investigate the early structural and dynamic changes that lead to the onset of the miscibility gap. Each temperature/ratio combination was simulated with 10 independent realizations of 150 ns with a time step of 2 fs and a frame-saving rate (for analysis) of 2 ps. To validate that our results from the small systems will be useful in describing the onset of the miscibility gap (i.e., confirm that the gap is at least approximately reproducible by the force field used in our simulations), we also perform three large (∼100 000 atom) simulations of a mixture of 0.4 THF/water (m/m) at 30, 90, and 165 °C (for at least 30 ns each) following the procedure (as outlined below) for the smaller systems.

Table 1. Simulation Sizes

mass ratio	no. of water molecules	no. of THF molecules	mole fraction
bulk water, 0 THF/water	1728[a]	0	1 water/water
bulk THF, 0 water/THF	0	360[b]	1 THF/THF
∼0.3 THF/water (m/m)	1658	125	0.07 THF/water
∼0.4 THF/water (m/m)	1250	125	0.09 THF/water
∼0.89 THF/water (m/m)	1119	250	0.183 THF/water
∼1.5 THF/water (m/m)	848	319	0.27 THF/water

[a]5184 atoms. [b]4680 atoms.

Systems were prepared in a three-step process: initial energy minimization, pressure relaxation, and a canonical (NVT) ensemble production run. Energy minimization was performed with the steepest-descent algorithm as implemented in the Gromacs 4.6 software package[23−27] to a tolerance of 100 kJ/(mol·nm). Pressure relaxation simulations (NPT) were performed for 2 ns at each temperature with the pressure fixed to 1 bar with the Berendsen barostat[28] and the temperature fixed with the V-Rescale thermostat.[29] Following pressure relaxation, the volume was taken to be fixed and the simulation protocol noted in the previous paragraph was followed (150 ns/simulation, 10 simulations per temperature/ratio pair) to generate production runs for analysis, with the V-Rescale thermostat used to maintain the required temperature. In both the pressure relaxation and production simulations, bonds were fixed with the LINCS[30,31] and SETTLE[32] algorithms.

Analysis Details. The structure and dynamics of the THF−water system were characterized by six metrics: center-of-mass radial distribution functions (RDFs), site-specific coordination numbers, spatial density functions, numbers of hydrogen bonds (HB), HB lifetimes, and diffusion constants. In addition, the RDFs were used to further calculate the second virial coefficient/pair interaction strengths (following the McMillan−Mayer formalism[33,34]). Each of these metrics was calculated at each temperature/ratio pair for each independent trajectory, with the average and standard error of the mean reported.

Coordination numbers were obtained by computing site−site radial distribution functions (obtained by use of the built-in Gromacs g_rdf utility) between the THF oxygen, H1−H4, and H2−H3 hydrogen atoms and water oxygen and hydrogen atoms, followed by integration up to the first minima. Figure 1 provides an illustration of our pair selections, and Table 2 reports the integration cutoffs used. The cutoffs correspond to the location of the first minima in the corresponding site−site radial distribution functions. Although the site−site radial distribution functions had to be computed in order to obtain these coordination numbers, the massive number of site−site functions (∼600 different plots) are difficult to view, and as such they are not presented.

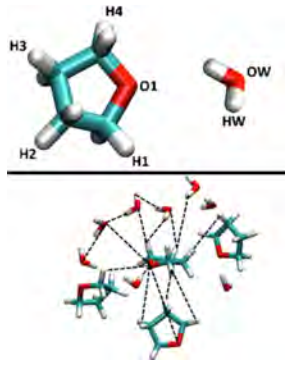

Figure 1. Visual representation of coordination sites. (Top) Labeled coordination sites. (Bottom) Examples of coordination. Dashed lines denote the different coordination pairs calculated.

Spatial densities were generated by selecting a random THF molecule and averaging over the entire simulation the count of

DOI: 10.1021/acs.jpcb.5b09770
J. Phys. Chem. B 2016, 120, 740−747

Table 2. Cutoffs for Coordination Number Calculations[a]

site 1	site 2	cutoff (nm)
THF−O1	water−OW	0.34
THF−O1	water−HW	0.25
THF−O1	THF−O1	0.53
THF−O1	THF−H1H4	0.38
THF−O1	THF−H2H3	0.36
THF−H1H4	water−OW	0.37
THF−H1H4	water−HW	0.41
THF−H1H4	THF−H1H4	0.31
THF−H1H4	THF−H2H3	0.32
THF−H2H3	water−OW	0.37
THF−H2H3	water−HW	0.51
THF−H2H3	THF−H2H3	0.35
water−OW	water−OW	0.37
water−OW	water−HW	0.25
water−HW	water−HW	0.31

[a]Cutoff = location of first minima in corresponding site−site RDFs at T = 30 °C.

water oxygen, water hydrogen, and THF ring atoms in bins of 1 Å^3 around the selected THF atom. This was achieved with the built-in GROMACS utility g_spatial. The average densities can then be represented as contours around a THF molecule for a visualization of the coordination around THF.

Hydrogen bonds and their lifetimes were computed by use of the built-in g_hbond utility from Gromacs. Hydrogen bonds were taken to be within donor−acceptor distances of 0.3 nm with a cutoff angle of 20°. Lifetimes were computed from the autocorrelation functions of each hydrogen bond, as described by Van der Spoel et al.[35]

Diffusion constants were obtained by measuring the mean-square displacement from each THF or water molecule at each time step and performing a linear regression from time step 15 000 (15 ns) to 135 000 (135 ns) for each realization. The mean diffusion constant value for each temperature/ratio pair (computed over all independent trajectories at that temperature/ratio pair) is reported along with the standard error of the mean (SEM).

The (osmotic) second virial coefficient/pair interaction strength is the following:

$$B_2 = -2\pi \int_0^\infty [e^{-w_2(r,z)/k_B T} - 1] r^2 \, dr \quad (1)$$

where r and $w_2(r, z)$ are the distance and the two-body potential of mean force (where z denotes that the potential mean force is being evaluated at a given activity). B_2 is a convenient measure of the self-interactions of the solution as a whole (the total second virial/two-body interaction strength) and between components (THF−THF, THF−water, and water−water). The theory behind the connection between the second virial coefficient of a liquid system and the two-body potential mean forces is well developed and documented.[33,34] Further, noting that if z is taken to be 0, the first term of integral of the equation above is equal to the radial pair distribution function, $g(r)$, we can quickly approximate the value of B_2 by simply integrating:

$$B_2 = -2\pi \int_0^\infty [g(r) - 1] r^2 \, dr \quad (2)$$

RESULTS

Coordination Numbers and Spatial Densities. Prior to discussing the calculated atomic coordination numbers it is of interest to note that the radial distribution functions (RDFs) between the centers of mass of THF and of the water molecules (see Figures S1−S6) were also calculated, and as expected, although changes in these quantities are seen with temperature (and detailed in the Supporting Information), it is not immediately clear how these minor changes are associated with the miscibility gap. Large-scale changes in structure are not evident in the center-of-mass RDFs, and the system has not yet phase-separated in the simulations. This is not surprising, as the system size (periodic box and number of molecules) was purposely chosen to be small (as noted in Computational Methods) to prevent a possible phase separation. To show that it is only a system size limitation that prevents us from observing large-scale phase separation and that the force field allows for a lower critical point, we performed three additional simulations, at 30, 90, and 165 °C (following the protocol in the Computational Methods section), of a system of ∼100 000 atoms, at a THF/H_2O ratio of ∼0.4. After 30 ns of simulation time has taken place, clear phase separation is found in the 90 °C system. However, no phase separation is observed at 30 °C (even after 75 ns of simulation) or at 165 °C (after 30 ns of simulation) (see Figure 2). These additional simulations clearly

Figure 2. Final configurations of large THF−water simulations (∼100 000 atoms): (left) 30 °C after 75 ns, (middle) 90 °C after 30 ns, and (right) 165 °C after 30 ns. Gray regions represent THF, while red indicates water.

indicate that the force field used can reproduce the miscibility gap (though the exact location of the critical points is not known for our model) and that it is that the small system size that limits our observation of a phase-separation event in the simulations.

In contrast to the RDFs, alterations in the coordination numbers (Figures 3−5) are more sensitive and do provide clear insight concerning local structural changes near the miscibility gap. Coordination numbers associated with THF−THF interactions (Figure 3) show a clear decrease with temperature, regardless of the THF concentration, and at each THF/H_2O ratio these trends are evident. Indeed, only two major alterations are found between the coordination numbers in bulk THF and those in the binary system: first, at low concentrations of THF the coordination between THF molecules is reduced (as expected), and second, the relative coordination number of H2H3−H2H3 pairs is increased at the cost of O1−H2H3 coordination.

As expected, water−water molecule coordination also decreases with increasing temperature (Figure 4). However, it is important to note that, in the presence of THF, the HW−HW coordination is found to be nearly the same as the OW−OW coordination for temperatures well beyond 75 °C (i.e., into the miscibility gap region). Indeed, at THF/H_2O (m/m) ratios beyond 0.31, the OW−OW and HW−HW coordination numbers are virtually the same up to temperatures of ∼120 °C

DOI: 10.1021/acs.jpcb.5b09770
J. Phys. Chem. B 2016, 120, 740−747

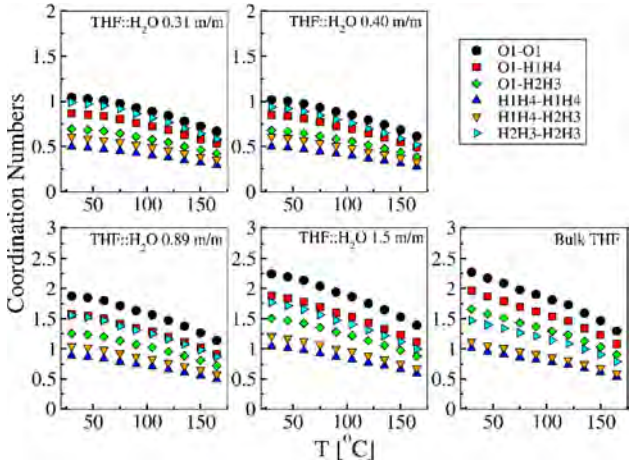

Figure 3. THF−THF coordination numbers. Error bars are the same size or smaller than the representative points and show the SEM.

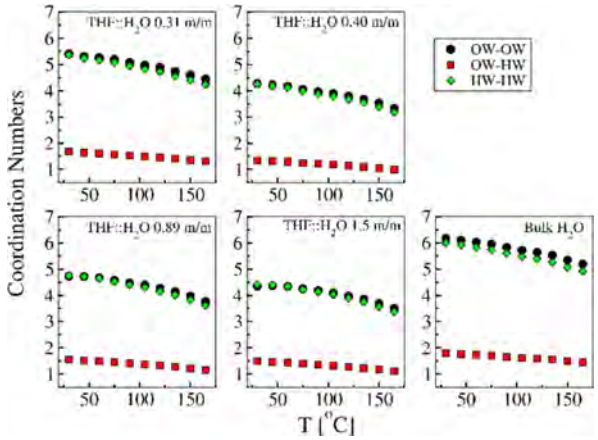

Figure 4. Water−water coordination numbers. Error bars are the same size or smaller than the representative points and show the SEM. A zoom-in of the black and green curves is provided in Figure S7 in Supporting Information for clarity.

(see Figure S7 for a "zoom-in" on the OW−HW coordination numbers).

THF−water coordination numbers (Figure 5 and Figure S8) show, as above, decreasing trends with increasing temperature. Unlike the case of THF−THF related coordination numbers, an inflection-point region, between ∼75 and ∼120 °C, is found for the H1H4−OW coordination number, indicating a decreased rate of structural change with temperature within this region. This is found at all concentrations, though it is most visible at 0.89 THF/H_2O (m/m) and weakest at 0.31 THF/H_2O (m/m) ratio.

Further insight into the structure is given by the average spatial density of atoms, which provides a three-dimensional visualization of the coordination of the solvent species. Figure 6 shows spatial densities of water oxygen atoms (red contours), water hydrogen atoms (blue), and THF ring atoms (orange) around a sample THF molecule at the four temperatures 30, 75, 120, and 165 °C for each concentration.

Consistent with the results from Figures 3−5, any coordination of THF is reduced, as all contours abate, with increasing temperature. The coordination of THF with other THF rings is shown to decrease at higher concentrations. Moreover, the hydrogen bond between the water hydrogen and

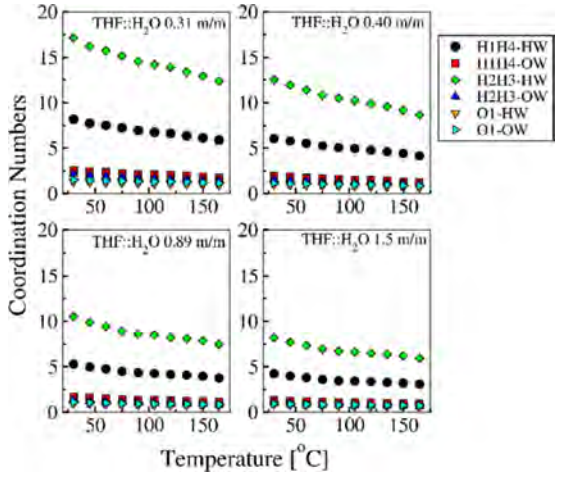

Figure 5. THF−water coordination numbers. Error bars are the same size or smaller than the representative points and show the SEM. Zoom-ins of the non-black and non-green curves are provided in Figure S8 in Supporting Information for clarity.

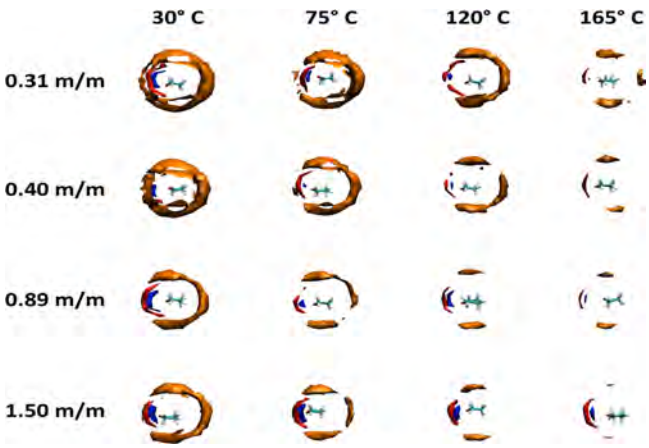

Figure 6. Spatial density functions. Orange corresponds to THF molecules, while red corresponds to water oxygen atoms and blue to water hydrogen atoms. The contours, representing regions of higher concentration, correspond to 1.5 times the concentration of water molecules and 1.25 times that of THF molecules in each system.

the O1 oxygen of THF is clearly depicted by the position, shape, and order of the red and blue contours.

Hydrogen Bonds. The numbers of hydrogen bonds (HBs) are shown in Figure 7 and the associated lifetimes in Figure 8. HBs between THF and water are found to be increased with increased concentration of THF (as one may expect) at the cost of water−water HBs. Despite a small loss of water−water HBs with increasing THF, water−water HBs still make up the majority of HBs in the simulations. An observation of additional interest is that the average total number of HBs that a water molecule makes at any given temperature is independent of the presence of THF; that is, the sum of the HBs between water molecules and THF and other water molecules in the THF binary system is nearly equal (within statistical error) to the number of HBs formed between water molecules in bulk water at the same temperature.

The HB lifetimes (Figure 8) clearly show that, in the presence of THF, water−water HBs are longer-lived (at low temperature they are nearly 5 times longer-lived at the highest THF concentration compared to bulk water). Under bulk

DOI: 10.1021/acs.jpcb.5b09770
J. Phys. Chem. B 2016, 120, 740−747

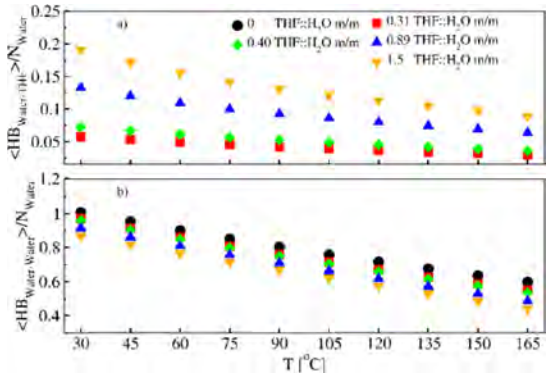

Figure 7. Average number of hydrogen bonds normalized by the number of water molecules: (a) THF−water and (b) water−water. Error bars are the same size or smaller than the representative points and show the SEM.

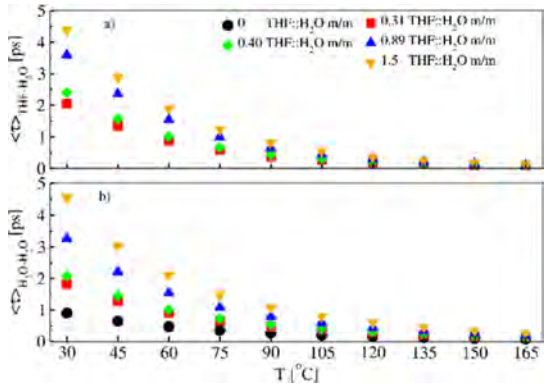

Figure 8. Mean HB lifetimes: (a) THF−water and (b) water−water. Error bars are the same size or smaller than the representative points and show the SEM.

conditions, average water−water HB lifetimes drop below 0.25 ps at temperatures above 75 °C; in contrast, at the lowest concentrations of THF [0.31 and 0.4 THF/H_2O (m/m)], water−water HB lifetimes do not drop below 0.25 ps until ∼105 °C is reached and not until a temperature between 120 and 135 °C is reached for the higher THF concentrations. Additional points of interest are that the water−water HB lifetimes become longer than those of THF−water with increasing temperature for the three highest THF concentrations and that the turnover temperature (the temperature at which the water−water HB lifetime dominates) is concentration-dependent, with turnover temperatures of 90, 75, and 60 °C for solutions with THF/H_2O mass fraction of 0.4, 0.89, and 1.5 (m/m), respectively.

Diffusion Constants. Diffusion constants of both THF and water are presented in Figure 9. What is unusual here is that while the diffusion constant of THF is largely invariant of concentration (i.e., regardless of concentration, the diffusion constant of THF increases linearly until ∼120 °C where the slope changes, followed by a "jump" at 165 °C), the diffusion constant of the water is both reduced compared to bulk and has a region of nonlinear increase. At the lowest and highest THF concentrations, the water diffusion is "slowed" between 75 and 135 °C. For the middle two THF concentrations, diffusion of water is increased. We also note that our bulk water diffusion constant measurement is consistent with that of Yeh and Hummer.[36]

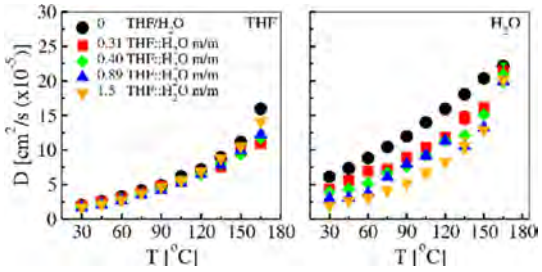

Figure 9. Solvent diffusion constants. Error bars are the same size or smaller than the representative points and show the SEM. Black circles show the diffusion constants of the noted species under bulk conditions.

Second Virial Coefficient/Pair Interaction Strengths. The behavior of the second virial coefficient/pair interaction strengths as a function of temperature is presented in Figures 10 and 11, with Figure 10 showing the composite (total

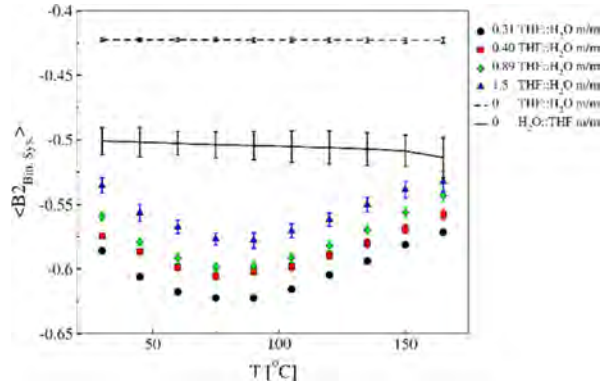

Figure 10. Mean system (total) second-virial coefficients. Error bars show the SEM, and those not immediately visible are at most the size of the symbol.

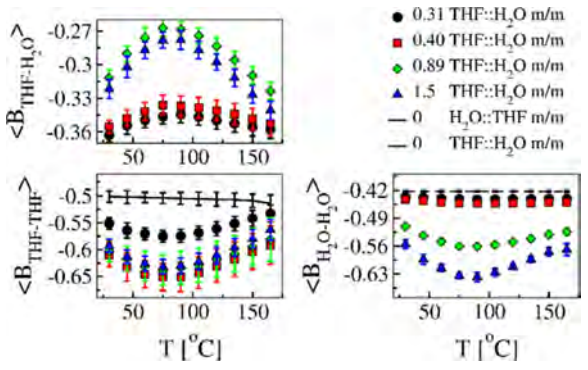

Figure 11. Individual components of the second virial coefficient. Error bars show the SEM, and those not immediately visible are at most the size of the symbol.

effective virial) and Figure 11 the THF−THF, water−water, and THF−water interaction virials. In both representations, the virials for the THF−water systems follow a near-parabolic trend with temperature, with the minimum at 90 °C, regardless of the THF/H_2O (m/m) ratio. Comparison of the binary systems to both bulk systems (THF and water) shows that all of the binary systems tested have a total virial significantly more negative at all temperatures below 165 °C than in bulk, consistent with a negative volume of mixing (as noted in the Introduction).

DOI: 10.1021/acs.jpcb.5b09770
J. Phys. Chem. B 2016, 120, 740−747

Turning to the components of the virial, it is of note that both the THF−THF and water−water virials are concave, while the THF−water virial is convex. Moreover, the THF−water coefficients are about two-thirds the magnitude of the water−water and THF values. An additional point of interest is that the THF−THF virial is nearly invariant with concentration when the mass ratio is above 0.3. Conversely, for systems with mass ratios above 0.4 (m/m), the water−water and the THF−water virials are significantly different from those at or below this value.

DISCUSSION

Using all-atom molecular dynamics, we examined the THF−water binary system at 10 different temperatures ranging from 30 to 165 °C and at six different mass ratios, two being the bulk limiting cases and four at ratios experimentally known to exhibit a miscibility gap at temperatures between 60 and 145 °C. The goal was to elucidate the structure and dynamics of the binary system at temperatures and concentrations associated with the experimental miscibility gap.

The small-scale changes in the simulations indicate that the temperature region associated with the miscibility gap is distinctive. From our results it is clear that the largest changes prior to the formal phase separation are found in the dynamics of the system and the second virial coefficient/pair interaction strength and are coupled with small changes in molecular coordination. Calculations of diffusion and second virial coefficients from the simulations show nonmonotonic (and, for the second virial, parabolic-like) behavior (or extrema in the case of the virial) in the temperature regime associated with the miscibility gap. Further, a crossover in HB lifetimes between water−water and THF−water occurs at temperatures associated with the miscibility gap for the three highest THF concentrations.

Recent work has shown that HB lifetimes have a strong influence on water self-diffusion, with longer lifetimes corresponding to slower diffusive behavior.[37] The present results at lower temperatures are consistent with this, and as our binary systems approach the miscibility gap, HB lifetimes are also modified and correspond with the anomalous trend in the diffusion constant. Considering that water is the only component of this binary system that can both donate and accept hydrogen bonds, it might seem reasonable to argue that water−water interactions are the most significant driver of the changes in the diffusion constant and likely the miscibility gap itself. If we follow this line of reasoning, we find supporting evidence in that the water−water coordination is altered, as noted by the increase in HW−HW coordination and its resilience to temperature, relative to bulk conditions. Additionally, the fact that the strength of the water−water virial is significantly larger (in magnitude) than that of the THF−water virial can also be taken as support.

However, the argument that only water−water interactions are strengthened within the miscibility gap is flawed, as THF also demonstrates minor coordination changes, for example, enhanced H2H3−H2H3 coordination, and a THF−THF interaction virial of similar strength to the water−water virial. Therefore, instead of the origin of the miscibility gap hinging on water−water interactions alone, the changes in THF behavior are indicative that THF also plays a role. Overall, the results suggest that the miscibility gap is the result of trends with temperature leading to mismatched interaction strength between the two components, which can be seen from an examination of the temperature trends in the computed virial components. The argument for the origin of the miscibility gap then would go as follows: as the temperature increases, the THF−water, THF−THF, and water−water interactions change at different rates (see Figure S9 for derivatives of the virial coefficient). As a result, THF−water interactions are lost, followed by the enhancement of either water−water or THF−THF interactions depending on concentration (and as a result of the increase in one self-interaction, the other would effectively see an increase, as it would be more prone to find interaction partners of the same type)

The above argument actually provides a correspondence between the increased diffusion of water for the middle two THF concentrations examined here and the decreases at the higher two concentrations. For the case of 0.4 THF/H_2O (m/m), while water−water interactions are largely unchanged, those for THF−THF increased, implying that THF has a stronger (and more attractive) interaction with itself than with water, and as a result it acts effectively as mildly repulsive to water (which has previously been shown to increase water diffusion),[38] as seen by the trend toward a positive THF−water virial. In the case of 0.89 THF/H_2O (m/m), the water−water attraction is increased in the gap [relative to values outside the gap and to the interaction terms computed for 0.3 and 0.4 THF/H_2O (m/m)]; however, in addition the THF−water interactions have become significantly more repulsive-like (closer to a positive virial). At the mass fraction of 1.5 THF/H_2O, water−water interactions are significantly stronger than THF−water and are on the order of THF−THF interactions, even at low temperatures (approximately 60 °C, which corresponds to the turnover point between THF−water HB lifetimes and water−water HB lifetime), and as a result the water diffusion is slowed. At the lowest concentration, water−water and THF−water interactions are nearly the same, and as a result water is slowed this time both by water−water HBs and by THF−water HBs (as noted by the lack of a turnover from THF−water to water−water dominant lifetimes for this lowest THF concentration).

Interestingly, the reasoning presented above also suggests how it is that the diffusion constant for THF is not significantly modified by concentration (at least for those tested here), as the THF−THF interactions are simply uniformly stronger than THF−water for all temperatures tested. Additionally, as THF molecules do not make hydrogen bonds, their diffusion is largely unaffected by an increased (relative to the miscible region) THF−THF attraction.

As a final comment on the above result, it is useful to consider previous theoretical work on systems with miscibility gaps, particularly the lattice model by Walker and Vause[39] (inspired by observations from Hirschfelder et al.[40]) and how our results fit into the larger picture of these types of systems. Walker and Vause[39] (and later Goldstein and Walker[41]) have been able to successfully describe binary systems with miscibility gaps using an Ising/Potts lattice model in which interactions between dissimilar pairs in a subset of configurations (Potts states) are favorable and interactions between similar pairs (THF−THF or water−water, for instance) are negligible or mildly favorable (dependent on the version of the model). In these models, as the temperature changes, the set of energetically accessible configurations (the associated degeneracy of the Potts states) is altered, and as a result the interaction strengths between the pairs (in our case THF−THF, water−water, and THF−water) also change with temperature. When

DOI: 10.1021/acs.jpcb.5b09770
J. Phys. Chem. B 2016, 120, 740−747

these interactions are altered by heating or cooling, the system exhibits a miscibility gap and the effective interaction strength near and within the miscibility gap follows a parabolic-like curve, which is consistent with the results presented here. Additionally, we observe a variety of small-scale coordination changes near the experimental miscibility gap region, which would support the supposed molecular mechanism behind the Walker and Vause model, that is, that there exist direction/state-specific interactions between the species.

CONCLUSIONS

This work has made use of all-atom molecular dynamics simulations to examine the structure and dynamics of the THF−water binary system near and within the immiscible region. The results suggest that the origin of the miscibility gap is the result of mismatched rates of change (with temperature) of many minor structure changes, which induce large changes to interaction strengths and produce pair interactions that have a parabolic temperature dependence.

ASSOCIATED CONTENT

Supporting Information

The Supporting Information is available free of charge on the ACS Publications website at DOI: 10.1021/acs.jpcb.5b09770.

Nine figures showing center-of-mass RDFs and secondary representations grouped by concentration, expanded views of Figures 4 and 5 in the main text, and derivatives of average components of the second-virial coefficient (PDF)

AUTHOR INFORMATION

Corresponding Author

*E-mail smithjc@ornl.gov.

Notes

The authors declare no competing financial interest.

ACKNOWLEDGMENTS

This research was funded by the BioEnergy Science Center, a U.S. Department of Energy (DOE) Bioenergy Research Center supported by the Office of Biological and Environmental Research in the DOE Office of Science. This research used resources of the Oak Ridge Leadership Computing Facility at the Oak Ridge National Laboratory, which is supported by the Office of Science of the U.S. Department of Energy under Contract DE-AC05-00OR22725. This research also used the computing resources provided by the U.S. Department of Energy's National Energy Research Scientific Computing Center. This paper has been authored by UT−Battelle, LLC under Contract DE-AC05-00OR22725 with the U.S. Department of Energy. The United States Government retains and the publisher, by accepting the article for publication, acknowledges that the United States Government retains a nonexclusive, paid-up, irrevocable, worldwide license to publish or reproduce the published form of this manuscript, or allow others to do so, for United States Government purposes. The Department of Energy will provide public access to these results of federally sponsored research in accordance with the DOE Public Access Plan (http://energy.gov/downloads/doe-public-access-plan).

REFERENCES

(1) Lai, S. T.; Sangermano, L.; Locke, D. C. Phenyl-Bonded Phase Liquid-Chromatography of Styrene Oligomers. *J. Chromatogr.* **1984**, *312* (Nov), 313−326.
(2) Theiler, S.; Hovetborn, T.; Keul, H.; Möller, M. Synthesis and Characterization of Amphiphilic Polyethers Based on Tetrahydrofuran and Glycidol: Antibacterial Assessment. *Macromol. Chem. Phys.* **2009**, *210* (8), 614−630.
(3) Naemura, K.; Ebashi, I.; Matsuda, A.; Chikamatsu, H. Enantiomer Recognition of Crown Ethers and Open-Chain Polyethers Containing the Trans-Tetrahydrofuran-2,5-Diylbis(Methylene) Subunit as the Chiral Center. *J. Chem. Soc., Chem. Commun.* **1986**, *9*, 666−668.
(4) Yoshida, S.; Suga, H.; Seki, S. Thermodynamic Studies of Solid Polyethers 0.3. Poly(Tetrahydrofuran), [-(Ch2)4o-]-/N. *Polym. J.* **1973**, *5* (1), 25−32.
(5) Cai, C. M.; Nagane, N.; Kumar, R.; Wyman, C. E. Coupling Metal Halides with a Co-Solvent to Produce Furfural and 5-Hmf at High Yields Directly from Lignocellulosic Biomass as an Integrated Biofuels Strategy. *Green Chem.* **2014**, *16* (8), 3819−3829.
(6) Cai, C. M.; Zhang, T. Y.; Kumar, R.; Wyman, C. E. Thf Co-Solvent Enhances Hydrocarbon Fuel Precursor Yields from Lignocellulosic Biomass. *Green Chem.* **2013**, *15* (11), 3140−3145.
(7) Lejcek, P.; Matous, J.; Novak, J. P.; Pick, J. Phase-Equilibria and Excess Molar Volumes of Tetrahydrofuran (1) + Deuterium-Oxide (2). *J. Chem. Thermodyn.* **1975**, *7* (10), 927−935.
(8) Matous, J.; Novak, J. P.; Sobr, J.; Pick, J. Phase Equilibria in the System Tetrahydrofuran(1)-Water(2). *Collect. Czech. Chem. Commun.* **1972**, *37*, 2653−2663.
(9) Bowron, D. T.; Finney, J. L.; Soper, A. K. The Structure of Liquid Tetrahydrofuran. *J. Am. Chem. Soc.* **2006**, *128* (15), 5119−5126.
(10) Bowron, D. T.; Finney, J. L.; Soper, A. K. Structural Characteristics of a 0.23 Mole Fraction Aqueous Solution of Tetrahydrofuran at 20 Degrees C. *J. Phys. Chem. B* **2006**, *110* (41), 20235−20245.
(11) Kiyohara, O.; Benson, G. C. Excess Enthalpies and Volumes of Water + Tetrahydrofuran Mixtures at 298.15k. *Can. J. Chem.* **1977**, *55* (8), 1354−1359.
(12) Mizuno, K.; Masuda, Y.; Yamamura, T.; Kitamura, J.; Ogata, H.; Bako, I.; Tamai, Y.; Yagasaki, T. Roles of the Ether Oxygen in Hydration of Tetrahydrofuran Studied by Ir, Nmr, and Dft Calculation Methods. *J. Phys. Chem. B* **2009**, *113* (4), 906−915.
(13) Bragg, A. E.; Kanu, G. U.; Schwartz, B. J. Nanometer-Scale Phase Separation and Preferential Solvation in Thf-Water Mixtures: Ultrafast Electron Hydration and Recombination Dynamics Following Ctts Excitation of I-. *J. Phys. Chem. Lett.* **2011**, *2* (21), 2797−2804.
(14) Critchfield, F. E.; Gibson, J. A.; Hall, J. L. Dielectric Constant and Refractive Index from 20 to 35-Degrees and Density at 25-Degrees for the System Tetrahydrofuran Water. *J. Am. Chem. Soc.* **1953**, *75* (23), 6044−6045.
(15) Oleinikova, A.; Weingartner, H. Isotope Effect on the Coexistence Curve and Crossover Behavior of Water Plus Tetrahydrofuran. *Chem. Phys. Lett.* **2000**, *319* (1−2), 119−124.
(16) Oleinikova, A.; Weingartner, H. Liquid-Liquid Coexistence Curves of Re-Entrant Phase Transitions Beyond the Asymptotic Range: Tetrahydrofuran Plus Water and Tetrahydrofuran Plus Heavy Water. *Phys. Chem. Chem. Phys.* **2002**, *4* (6), 955−962.
(17) Brovchenko, I.; Guillot, B. Simulation of the Liquid-Liquid Coexistence of the Tetrahydrofuran Plus Water Mixture in the Gibbs Ensemble. *Fluid Phase Equilib.* **2001**, *183-184*, 311−319.
(18) Oleinikova, A.; Brovchenko, I.; Geiger, A.; Guillot, B. Percolation of Water in Aqueous Solution and Liquid-Liquid Immiscibility. *J. Chem. Phys.* **2002**, *117* (7), 3296−3304.
(19) Vorobyov, I.; Anisimov, V. M.; Greene, S.; Venable, R. M.; Moser, A.; Pastor, R. W.; MacKerell, A. D. Additive and Classical Drude Polarizable Force Fields for Linear and Cyclic Ethers. *J. Chem. Theory Comput.* **2007**, *3* (3), 1120−1133.
(20) Jorgensen, H.; Kristensen, J. B.; Felby, C. Enzymatic Conversion of Lignocellulose into Fermentable Sugars: Challenges and Opportunities. *Biofuels, Bioprod. Biorefin.* **2007**, *1* (2), 119−134.

DOI: 10.1021/acs.jpcb.5b09770
J. Phys. Chem. B 2016, 120, 740−747

(21) Binder, K. Reply to 'Comment on "Theory of the Evaporation/Condensation Transition of Equilibrium Droplets in Finite Volumes"'. *Phys. A* **2003**, *327* (3−4), 589−592.
(22) Binder, K. Theory of the Evaporation /Condensation Transition of Equilibrium Droplets in Finite Volumes. *Phys. A* **2003**, *319*, 99−114.
(23) Abraham, M. J.; Gready, J. E. Optimization of Parameters for Molecular Dynamics Simulation Using Smooth Particle-Mesh Ewald in Gromacs 4.5. *J. Comput. Chem.* **2011**, *32* (9), 2031−2040.
(24) Van der Spoel, D.; Lindahl, E.; Hess, B.; Groenhof, G.; Mark, A. E.; Berendsen, H. J. C. Gromacs: Fast, Flexible, and Free. *J. Comput. Chem.* **2005**, *26* (16), 1701−1718.
(25) Bekker, H.; Berendsen, H. J. C.; Dijkstra, E. J.; Achterop, S.; Vondrumen, R.; Vanderspoel, D.; Sijbers, A.; Keegstra, H.; Reitsma, B.; Renardus, M. K. R. Gromacs - a Parallel Computer for Molecular-Dynamics Simulations. *Physics Computing '92*, 1993, pp 252−256.
(26) Hess, B.; Kutzner, C.; van der Spoel, D.; Lindahl, E. Gromacs 4: Algorithms for Highly Efficient, Load-Balanced, and Scalable Molecular Simulation. *J. Chem. Theory Comput.* **2008**, *4* (3), 435−447.
(27) Pronk, S.; Pall, S.; Schulz, R.; Larsson, P.; Bjelkmar, P.; Apostolov, R.; Shirts, M. R.; Smith, J. C.; Kasson, P. M.; van der Spoel, D.; Hess, B.; Lindahl, E. Gromacs 4.5: A High-Throughput and Highly Parallel Open Source Molecular Simulation Toolkit. *Bioinformatics* **2013**, *29* (7), 845−854.
(28) Berendsen, H. J. C.; Postma, J. P. M.; Vangunsteren, W. F.; Dinola, A.; Haak, J. R. Molecular-Dynamics with Coupling to an External Bath. *J. Chem. Phys.* **1984**, *81* (8), 3684−3690.
(29) Bussi, G.; Donadio, D.; Parrinello, M. Canonical Sampling through Velocity Rescaling. *J. Chem. Phys.* **2007**, *126*, No. 014101, DOI: 10.1063/1.2408420.
(30) Hess, B. P-Lincs: A Parallel Linear Constraint Solver for Molecular Simulation. *J. Chem. Theory Comput.* **2008**, *4* (1), 116−122.
(31) Hess, B.; Bekker, H.; Berendsen, H. J. C.; Fraaije, J. G. E. M. Lincs: A Linear Constraint Solver for Molecular Simulations. *J. Comput. Chem.* **1997**, *18* (12), 1463−1472.
(32) Miyamoto, S.; Kollman, P. A. Settle - an Analytical Version of the Shake and Rattle Algorithm for Rigid Water Models. *J. Comput. Chem.* **1992**, *13* (8), 952−962.
(33) Hill, T. L. *Statistical Mechanics: Principles and Selected Applications*; Dover Publications, 1987 (reprint of the McGraw-Hill Book Co., Inc., 1956 edition).
(34) McMillan, W. G., Jr.; Mayer, J. E. The Statistical Thermodynamics of Multicomponent Systems. *J. Chem. Phys.* **1945**, *13* (7), 276−305.
(35) van der Spoel, D.; van Maaren, P. J.; Larsson, P.; Timneanu, N. Thermodynamics of Hydrogen Bonding in Hydrophilic and Hydrophobic Media. *J. Phys. Chem. B* **2006**, *110* (9), 4393−4398.
(36) Yeh, I. C.; Hummer, G. System-Size Dependence of Diffusion Coefficients and Viscosities from Molecular Dynamics Simulations with Periodic Boundary Conditions. *J. Phys. Chem. B* **2004**, *108* (40), 15873−15879.
(37) Zhang, N.; Li, W. Z.; Chen, C.; Zuo, J. G.; Weng, L. D. Molecular Dynamics Study on Water Self-Diffusion in Aqueous Mixtures of Methanol, Ethylene Glycol and Glycerol: Investigations from the Point of View of Hydrogen Bonding. *Mol. Phys.* **2013**, *111* (7), 939−949.
(38) Srinivas, G.; Bhattacharyya, S.; Bagchi, B. Computer Simulation and Mode Coupling Theory Study of the Effects of Specific Solute-Solvent Interactions on Diffusion: Crossover from a Sub-Slip to a Super-Stick Limit of Diffusion. *J. Chem. Phys.* **1999**, *110* (9), 4477−4482.
(39) Walker, J. S.; Vause, C. A. Theory of Closed-Loop Phase-Diagrams in Binary Fluid Mixtures. *Phys. Lett. A* **1980**, *79* (5−6), 421−424.
(40) Hirschfelder, J.; Stevenson, D.; Eyring, H. A Theory of Liquid Structure. *J. Chem. Phys.* **1937**, *5* (11), 896−912.
(41) Goldstein, R. E.; Walker, J. S. Theory of Multiple Phase Separations in Binary-Mixtures - Phase-Diagrams, Thermodynamic Properties, and Comparisons with Experiments. *J. Chem. Phys.* **1983**, *78* (3), 1492−1512.

DOI: 10.1021/acs.jpcb.5b09770
J. Phys. Chem. B 2016, 120, 740−747